UC San Diego
UC San Diego Previously Published Works

Title

Aggregation Temperature of Escherichia coli Depends on Steepness of the Thermal Gradient

Permalink

https://escholarship.org/uc/item/9kc5z0mp

Journal

Biophysical Journal, 118(11)

ISSN

0006-3495

Authors

Yang, Chih-Yu
Erickstad, Michael
Tadrist, Loïc
et al.

Publication Date

2020-06-01

DOI

10.1016/j.bpj.2020.02.033

Peer reviewed

Aggregation Temperature of *Escherichia coli* Depends on Steepness of the Thermal Gradient

Chih-Yu Yang,[1] Michael Erickstad,[1] Loïc Tadrist,[1] Edward Ronan,[1] Edgar Gutierrez,[1] Jérôme Wong-Ng,[1,*] and Alex Groisman[1,*]

[1]Department of Physics, University of California, San Diego, La Jolla, California

ABSTRACT   Bacterial chemotaxis, the directed migration of bacteria in a gradient of chemoattractant, is one of the most well-studied and well-understood processes in cell biology. On the other hand, bacterial thermotaxis, the directed migration of bacteria in a gradient of temperature, is understood relatively poorly, with somewhat conflicting reports by different groups. One of the reasons for that is the relative technical difficulty of the generation of well-defined gradients of temperature that are sufficiently steep to elicit readily detectable thermotaxis. Here, we used a specially designed microfluidic device to study thermotaxis of *Escherichia coli* in a broad range of thermal gradients with a high rate of data collection. We found that in shallow temperature gradients with narrow temperature ranges, *E. coli* tended to aggregate near a sidewall of the gradient channel at either the lowest or the highest temperature. On the other hand, in sufficiently steep gradients with wide temperature ranges, *E. coli* aggregated at intermediate temperatures, with maximal cell concentrations found away from the sidewalls. We observed this intermediate temperature aggregation in a motility buffer that did not contain any major chemoattractants of *E. coli*, in contradiction to some previous reports, which suggested that this type of aggregation required the presence of at least one major chemoattractant in the medium. Even more surprisingly, the aggregation temperature strongly depended on the gradient steepness, decreasing by ∼10° as the steepness was increased from 27 to 53°C/mm. Our experiments also highlight the fact that assessments of thermal gradients by changes in fluorescence of temperature-sensitive fluorescent dyes need to account for thermophoresis of the dyes.

SIGNIFICANCE   A difference between thermotaxis and other types of directed cell migration is that, in their search for optimal conditions, cells are expected to nearly equally avoid both low and high temperatures and to aggregate at an intermediate temperature. Relatively few experimental studies of thermotaxis have been performed, partly because of technical difficulties of exposing live cells to controlled thermal gradients. Here, we designed and used a microfluidic experimental setup, imposing various thermal gradients on motile *Escherichia coli* cells. When exposed to a sufficiently broad temperature range and steep gradient, *E. coli* cells aggregated at an intermediate temperature. Surprisingly, the aggregation temperatures significantly decreased with the steepness of the thermal gradient, an effect that was neither predicted nor observed before, to our knowledge.

INTRODUCTION

Motile bacteria are capable of sensing and responding to a variety of environmental cues. A paradigm for such responses is the chemotaxis of *Escherichia coli* in spatial gradients of soluble chemoattractants, a behavior guiding *E. coli* toward regions with greater concentrations of various nutrients and, hence, improved growth conditions. *E. coli* chemotaxis is physically achieved through a combination of smooth swimming and tumbling, which are tied to two different states of cellular flagellar motors. During smooth swimming streaks, a cell keeps swimming in a certain direction, whereas tumbling results in a change in the swimming direction. When a cell moves up the gradient of an attractant, the concentration of the attractant around the cell increases with time, making the intervals of smooth swimming longer and the tumbling events less frequent (1,2). The resulting migration of a cell can be reasonably modeled by a biased random walk, with the bias being provided by the gradient of attractant and increasing with steepness of the gradient (3,4). The frequency of tumbling is controlled through histidine kinase CheA, whose activity is inhibited when the concentration of attractant increases

in time ([5–7]). CheA phosphorylates the response regulator CheY, which, in its active phosphorylated state, tends to induce tumbling. Dephosphorylation of CheY by the phosphatase CheZ, which is usually constitutively active, leads to smooth swimming. The fact that chemotaxis of *E. coli* depends on temporal changes in the local concentration of attractant, as experienced by a moving cell, has greatly facilitated studies of the underlying molecular signaling networks. Instead of setting up spatial gradients of an attractant and observing the migration of *E. coli* cells in them, cells are tethered to a substrate by a single flagellum and exposed to stepwise changes in the concentration of the attractant, and the resulting changes in the dynamics of rotation of the flagellum are monitored. In addition, *E. coli* cells have been immobilized on substrates, and their responses to stepwise changes of attractant have been monitored using Förster resonance energy transfer (FRET) microscopy and fluorescently labeled CheY and CheZ, with a stronger FRET signal indicating a higher level of activity of CheY ([8]).

Other major types of directed migration of *E. coli* (and many other bacteria) toward regions with better growth conditions are aerotaxis (oxygen taxis), pH taxis, and thermotaxis that, respectively, occur in response to gradients of oxygen tension, pH, and temperature. Aerotaxis is similar to chemotaxis in gradients of nutrients in the sense that it is largely unidirectional because both greater nutrient concentration and greater oxygen concentrations are usually beneficial (*E. coli* is repelled from oxygen concentrations above the atmospheric level of $\sim$21% ([9]), but there is no clear evidence of repulsion from physiological levels of oxygen ([10])). Both pH taxis and thermotaxis are essentially different, however. *E. coli* favor a near-neutral pH of $\sim$7.5 and are repelled by excessively acidic or alkaline pH environments that are detrimental for *E. coli* growth ([11,12]). The optimal temperature for *E. coli* growth is usually considered to be 35–40°C. The *E. coli* growth rate (in rich medium) is very low below 10°C, gradually increases to $\sim$25% of the maximum at room temperature, reaches the maximum at 35–40°C, and precipitously drops above 42°C to as little as 10% of the maximum at 47°C and to nearly zero at 50°C.

Given the pH preferences of *E. coli*, it is reasonable to assume that, if placed into a spatial gradient of pH, *E. coli* would aggregate at pH $\sim$7.5. The FRET biosensor data on the responses of immobilized *E. coli* to stepwise changes in pH are suggestive of such aggregation. It has not been shown directly, however (there is direct evidence of aggregation of *Serratia marcescens*, another motile Gram-negative bacteria, at intermediate pH in a spatial gradient of pH ([13])). Similarly, it is reasonable to assume that, if placed in a temperature gradient, *E. coli* would aggregate at 35–40°C. The responses of tethered *E. coli* (in terms of changes in the direction of flagellum rotation) to short 3°C positive pulses of the ambient temperature indicated that *E. coli*

are thermophilic (warm-seeking) at temperatures below 37°C and cryophilic (cold-seeking) above 37°C ([14]). This result suggests that in a temperature gradient, free-swimming *E. coli* should aggregate at $\sim$37°C.

Nevertheless, until recently ([15]) there has been no clear experimental evidence of aggregation of *E. coli* at an intermediate temperature in a gradient by means of thermotaxis, and studying *E. coli* thermotaxis has proved to be difficult in general. One of the reasons is that the two receptors that are commonly considered to be primarily responsible for temperature sensing in *E. coli*, Tsr and Tar ([15–19]), are methyl-accepting chemotaxis protein (MCP) chemoreceptors, which are most abundant in *E. coli*, have strong affinities to serine and aspartate, respectively, and are also sensitive to a variety of other chemoattractants. As a result, the response of Tsr and Tar to temperature changes strongly depends on the concentrations of serine and aspartate in the medium and can be completely suppressed or even reversed (in terms of the effect of temperature changes on the smooth swimming time), when the concentration of attractants is increased ([15,18]). At a given temperature and medium composition, the responses of the Tsr and Tar receptors to a temperature change may be opposite (with one enhancing the activity of CheA and the other suppressing it), and the outcome may be decided by the relative abundance of the two receptors. This relative abundance is generally variable, and, for *E. coli* grown in an exponential culture, the Tar/Tsr ratio has been reported to increase by as much as an order of magnitude between OD_{600} of 0.1 and 0.5 ([15,18]). Hence, the results of a thermotaxis experiment depend on the stage of growth reached by cells used in the experiment, and to make the results consistent, it is essential to always grow and prepare cells in the same way. In addition, temperature sensitivity has also been reported for two other MCP receptors, Trg and Tap ([20]), as well as for Aer ([21]), which is primarily responsible for aerotaxis.

Another inherent difficulty in the studying of thermotaxis is that temperature has major effects on *E. coli* physiology, affecting their rate of growth, metabolism, and respiration, as well as the speed of swimming, v, and the characteristic time between consecutive tumbling events, τ ([22,23]). So, when *E. coli* cells are exposed to a temperature gradient for a long time, especially in a nutrient-rich medium, their concentration distributions may become uneven because of the different growth rates at different temperatures. In addition, a temperature gradient may generate a nutrient gradient by thermophoresis ([24,25]), and this nutrient gradient may cause chemotaxis that would manifest as thermotaxis, without involving any direct bacterial temperature sensing ([4,26]). Furthermore, spatial variations in the rates of consumption of nutrients and respiration, especially at high cell densities, may lead to gradients of chemoattractants and oxygen, causing chemotaxis and aerotaxis ([26]). To avoid or at least minimize these

secondary effects, it is preferable to perform experiments at a small cell density, in a motility buffer or minimal medium, and in a setup in which thermotactic response can be measured within a short time interval (as compared with the timescale of changes in *E. coli* physiology or medium composition due to exposure to high and low temperatures, nutrient depletion, etc.).

In the absence of directional bias, the movement of *E. coli* can be modeled by diffusion with an effective coefficient $D = \tau v^2$ (3,4). Hence, if *E. coli* are placed in a compartment with a size w, their spatial distribution is expected to reach a steady state after a time $t_d = w^2/(2D) = w^2/(2\tau v^2)$. The steady-state distribution depends on the bias in *E. coli* swimming. However, the time to reach this distribution is independent of the bias as long as the bias remains sufficiently small, which is nearly always the case. Therefore, if the readout of a thermotaxis assay is the shape of the steady-state spatial distribution of *E. coli* in a certain temperature gradient, a time of at least t_d should be allowed after the exposure of *E. coli* to the gradient before reliable measurements of the steady-state distribution can be taken. Importantly, the time t_d increases as w^2. With the characteristic values of v and τ at ~ 20 μm/s and ~ 1 s, respectively, the characteristic value of D is ~ 400 μm^2/s, corresponding to t_d of ~ 2 min, ~ 20 min, and ~ 3 h for $w = 0.3$, 1.0, and 3.0 mm, respectively. The time of 20 min is a physiological scale corresponding to the doubling time of *E. coli* in an optimal medium at 37°C. Therefore, to minimize changes in *E. coli* physiology in a thermotaxis assay, in which the readout is the steady-state distribution in a temperature gradient, it is preferable to limit the size of the compartment with the gradient to $L < 1$ mm (especially if the gradient spreads over temperatures around 37°C).

In a number of studies on *E. coli* thermotaxis (22,26–28), the temperature gradient profiles spread over lengths on the order of 10 mm, leading to times t_d on the order of ~ 30 h and to relatively shallow temperature gradients in a range of 2.2–3.5°C/mm. As a result, the distributions of *E. coli* concentration across the gradient profile continued evolving over the course of the experiments (>1 h), and the shapes of these evolving distributions were, most likely, affected by factors other than the inherent warm-seeking or cold-seeking behavior of individual cells. Among those factors are gradually developing spatial nonuniformity of the nutrient content and oxygen tension (27) due to different cumulative rates of cellular metabolism and respiration at different temperatures and different cell concentrations and due to temperature dependences of the swimming speed, v, and persistence time, τ. A temperature dependence of v can lead to an effective directed migration of cells in thermal gradients (4), which does not require the receptors Tsr and Tar that are engaged in the classical thermotaxis (22). When v is position dependent, the steady-state local density of bacteria is expected to be proportional to $1/v$

(4). The variation of v with temperature depends on composition of the medium. It can reach a factor of 2 between 20 and 40°C and can lead to a migration of *E. coli* toward higher or lower temperatures (22).

Thermotaxis-driven aggregation of *E. coli* at intermediate temperatures was recently reported by Yoney and Salman (15), who generated nonlinear axisymmetric temperature gradients by heating water in a microchannel with an infrared laser. The gradients were much sharper than in the previous literature, with the reported temperature increasing from 30 to 55°C over 100 μm, eliciting rapid changes in the spatial distribution of *E. coli*. The experiments were performed in a nutrient-rich M9CG medium at a relatively high cell density (OD of 0.3), and the aggregation temperature was reported to depend on the density the cells were grown to in an exponential culture before the thermotaxis assay (and, hence, the Tar/Tsr receptor ratio) (15). On the other hand, no aggregation at intermediate temperatures was observed for cells in motility buffer (15). Therefore, it cannot be completely ruled out that the intermediate temperature aggregation in the M9CG medium was at least partly caused by chemotaxis that was elicited by a nutrient gradient generated by thermophoresis in the temperature gradient.

Another recent study of the *E. coli* thermotaxis (29) combined intracellular signaling experiments using FRET microscopy with stepwise changes in temperature in different media, mathematical modeling, and microfluidic experiments with an earlier version of the device used in our article. This study was focused on the signal transduction through the Tsr and Tar receptors. The main conclusion of this study was that the thermotactic aggregation of *E. coli* at an intermediate temperature in a gradient requires the presence of both Tsr and Tar, which are largely interchangeable, and occurs when either one, but not both, of the receptors is stimulated with its specific chemoattractant (serine and aspartate, respectively). This study also suggested that thermotactic aggregation cannot occur in a motility buffer and in the absence of chemoattractants for Tsr and Tar, in general.

Microfluidic technologies have been successfully used to study bacterial chemotaxis (30). Notably, Kalinin et al. used microfluidic devices with microchannels cast in hydrogel to perform detailed studies of *E. coli* chemotaxis in a variety of well-defined linear gradients (31). The studies highlighted the large range of ambient concentrations of attractant to which *E. coli* can adapt and indicated that it is more appropriate to interpret *E. coli* chemotaxis as the sensing of fractional (logarithmic) rather than absolute concentration changes. A conceptually new type of directed migration assay enabled by microfluidics is to continuously perfuse a suspension of swimming cells through a long channel with a gradient of a migration-eliciting factor applied across the channel (32). If the cross-channel gradient does not change with the position along this gradient channel and

the residence time of cells in it is longer than the diffusion time $w^2/(2D)$, where w is the channel width, the cross-channel distribution of cells at the downstream end of the gradient channel is expected to represent their steady-state distribution in the gradient. An advantage of this approach is that the continuous perfusion makes it possible to collect data on large numbers of individual cells, with the data collection done continuously, without changing anything in the experimental setup.

This type of assay is difficult to implement for chemotaxis because cross-channel gradients of the common chemoattractants are normally set at the beginning (upstream end) of the gradient channel and gradually change along the channel because of molecular diffusion (32). On the other hand, the continuous flow assay was successfully implemented for aerotaxis (10). Stable linear cross-channel gradients of oxygen were generated by the diffusion of oxygen through the porous microfluidic device between two parallel gas-filled channels, which flanked the liquid-filled gradient channel with *E. coli* and functioned as a source and sink. A somewhat analogous approach was used to generate gradients of temperature in a microfluidic device (33). Warm and cold water were circulated at relatively high rates through two large-cross-sectional parallel channels, which served as the source and sink of heat and created a near-linear gradient of temperature across the strip between them (cf. Fig. 1; (33)).

Here, we performed a series of experiments observing *E. coli* thermotaxis in various linear gradients of temperature using a microfluidic device (Fig. 1 *A*) that combines elements from the devices of (10,33). Two parallel channels with hot and cold water flank a 500-μm gradient channel through which a suspension of *E. coli* is slowly perfused, generating a stable linear gradient of temperature across the gradient channel. A new element of the device is a cell motility filter, also known as H-filter (34) (*magnified view* in Fig. 1 *A*), which is added upstream of the gradient channel and makes it possible to exclude nonmotile cells from the thermotaxis assays (Fig. S1). Importantly, experiments were performed in a motility buffer with glycerol as the energy source and at a low cell density (OD $\sim$0.03), and the value of t_d across the channel was only $\sim$5 min. This experimental setup was designed to minimize the secondary chemotaxis effects, effects of the medium composition upon the thermal responses of the Tsr and Tar receptors, and long-term temperature-induced changes in the *E. coli* physiology. When the temperature gradients covered sufficiently broad ranges, we consistently observed distinct peaks in cross-channel distributions of *E. coli* density, which appeared in an internal region of the gradient channel, indicating aggregation at intermediate temperatures. To our surprise, however, as the gradients became sharper, the aggregation temperatures steadily decreased from $\sim$40°C for a gradient of 27°C/mm to as low as $\sim$30°C for 53°C/mm.
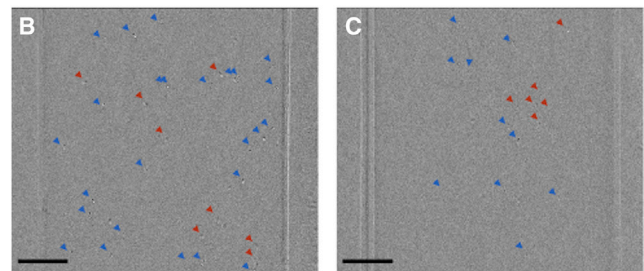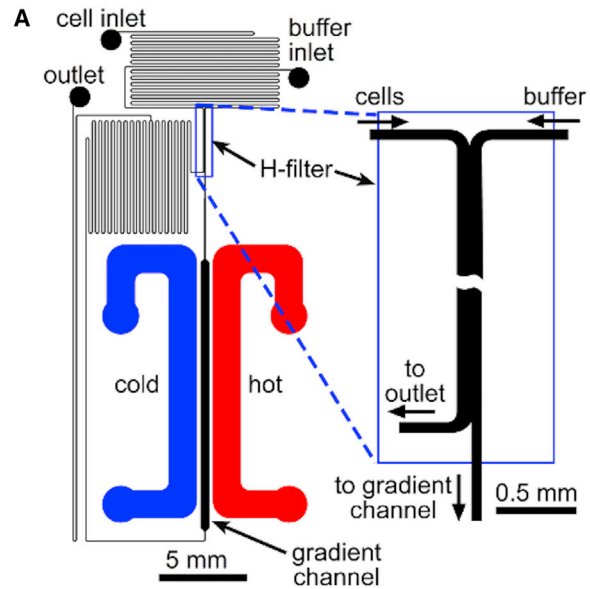

FIGURE 1 Microfluidic device for experiments on bacterial thermotaxis. (*A*) The drawing of the channels shows a network of 100-μm-deep interconnected microchannels (shown in *black*), to which an *E. coli* suspension is supplied, and two separate 1-mm-deep channels, through which hot and cold water is circulated (shown in *red* and *blue*, respectively). The network of 100-μm-deep microchannels has two inlets for a cell suspension and motility buffer and one outlet. A near-linear temperature profile is generated in the gradient channel, which is flanked by the two water circulation channels. A magnified view of another key element of the microchannel network, the H-filter, which prevents nonmotile cells from entering the gradient channel, is shown on the right. (*B*) and (*C*) show images of *E. coli* cells at the midplane of the gradient channel near the upstream and downstream end, respectively. Each of the images resulted from digital subtraction of two consecutive micrographs taken with an $\sim$133-ms interval. The subtraction suppresses the static background and emphasizes changes due to moving cells. Blue arrows point to sharp images of cells (cells within the depth of field of the video microscope), which are picked up and validated by the MATLAB code, and red arrows point to blurred images of cells (out of focus), which are disregarded (because the contrast is below the threshold). Scale bars, 100 μm. The temperatures at the left and right walls of the gradient channel (T_l and T_r) are 26 and 43°C, respectively. The total number of cells at the channel midplane was always smaller at the downstream end, which was likely due to cell sedimentation and residual sticking of cells to the glass substrate and to the channel walls. To see this figure in color, go online.

MATERIALS AND METHODS

Bacterial culture

Thermotaxis experiments were performed on an *E. coli* strain RP437 (with streptomycin resistance). Cells from a single colony in an LB agar plate

were grown overnight in TB (10 g/L Bacto Tryptone, 5 g/L NaCl, in H_2O) with streptomycin (100 μg/mL) at 34°C, to prevent contamination. 50 μL of the overnight culture was then added to 5 mL TB and grown to OD_{600} of ~0.24 ± 0.02 (~2.5 h). Cells were washed three times and resuspended in a motility buffer (10 mM potassium phosphate, 0.1 mM EDTA, 50 mM glycerol, and 1 μM L-methionine (pH 7.0)) via centrifugation at 3600 rpm for 11 min. The final OD was adjusted to OD_{600} ~0.1 ± 0.01, and the suspension was immediately fed to the microfluidic device.

Microfluidics and flow setup

The microfluidic device used in the thermotaxis experiments (Fig. 1) is made of a microfabricated monolithic polydimethylsiloxane chip sealed with a #1.5 microscope cover glass. The device has a network of 100-μm deep microchannels and two separate 1-mm deep channels. The 100-μm deep microchannel network has two inlets, a cell inlet and a buffer inlet, and a single outlet. The main element of this network is a rectilinear gradient channel, which has a length of 15 mm and a width $w = 500$ μm and across which the temperature gradients are applied. The bacterial suspension is fed to the cell inlet and is perfused through the gradient channel toward the outlet at a mean flow velocity $v_{fl} \approx 30$ μm/s. Along ~13.5 mm of its length, the gradient channel is flanked by the two 1-mm deep channels, which are $d = 834$ μm apart from each other (with 167-μm partitions between them and the gradient channel) and are both 1.6 mm wide. The circulation of cold water, with a temperature T_c, through the 1-mm-deep channel on the left and hot water, with a temperature T_h, through the 1-mm channel on the right creates a near-linear temperature profile across the gradient channel with a slope of ~$(T_h - T_c)/d$. This technique of on-chip generation of a temperature gradient and this general layout of the device are adapted from a previous publication (33).

To account for the edge effects at the upstream and downstream ends of the gradient channel, where the gradient channel is no longer flanked by the two water circulation channels, we performed three-dimensional numerical simulations of temperature distribution profiles in Comsol. The simulations indicated that the temperature gradient across the gradient channel remains unchanged (within the precision of the simulations or ~2%) along a gradient channel segment with a length $L = 11$ mm. The distribution of *E. coli* across the gradient channel is expected to reach a steady state after a time $t_d = w^2/(2D) = 310$ s (where, as before, $D = 400$ μm^2/s is the effective diffusion coefficient of motile *E. coli*). This time is substantially shorter than the residence time of bacteria in the segment of the gradient channel with a constant temperature gradient, $t_{res} = L/v_{fl} = 367$ s. Therefore, the distribution of *E. coli* across the gradient channel measured near its downstream end is expected to represent their steady-state distribution in the temperature gradient.

The flow through the 100-μm-deep microchannel network is driven and controlled by the application of ~200 Pa differential pressure between the two inlets and the outlet. To this end, the liquids in the reservoirs connected to the inlets were held at a level of ~2 cm above the level of the liquid in the reservoir connected to the outlet (all three reservoirs were modified 1.7 mL Eppendorf tubes). The experimental setup and microfluidic device are conceptually similar to those that we previously used to study the aerotaxis of *E. coli* (10). However, the thermotaxis device has an additional element, an H-filter (34), that is a channel with a width $w_h = 150$ μm and length $L_h = 3.5$ mm located upstream of the gradient channel, serving to prevent nonmotile *E. coli* from reaching the gradient channel (Fig. 1 *A*). The left and right sides of the H-filter inlet (upstream end) are connected, respectively, to the buffer and cell inlets of the device. At the outlet, the left and right sides of the H-filter channel are connected, respectively, to the gradient channel and the device outlet, with 1/3 of the stream directed toward the gradient channel and the remaining 2/3 directed toward the device outlet (through a dedicated bypass channel line). The 1:2 split is set by the resistance channel. Under normal operating conditions, the motility buffer and bacterial suspension are fed to the H-filter inlet at a flow rate ratio of ~1:1 (controlled through the pressures at the two inlets). Hence, in the

absence of bacterial motility (which leads to diffusion-like spreading), the entire stream of the bacterial suspension is directed toward the bypass line and does not enter the gradient channel (Fig. S1). The mean flow velocity in the H-filter channel is $v_h \approx 300$ μm/s, corresponding to a residence time $L_h/v_h = 12$ s, which is comparable to the effective cross-channel diffusion time for motile *E. coli*, $w_h^2/(2D) = 28$ s. Therefore, at the H-filter outlet, motile *E. coli* are broadly distributed across the channel, and a substantial portion of them enter the gradient channel (Fig. S1). An estimate, ignoring the nonuniformity of the flow velocity over the channel cross section, suggests that when bacterial suspension and motility buffer are fed to the H-filter at 1:1 ratio, no nonmotile cells and as many as 30% of motile cells are directed toward the gradient channel. On the way between the outlet of the H-filter and the inlet of the gradient channel, motile *E. coli* then become nearly uniformly distributed across the channel width.

In addition to enabling the positive selection for motile *E. coli*, the H-filter also makes it possible to adjust the concentration of bacterial suspension in the gradient channel. When the flow rate ratio between the bacterial suspension and motility buffer at the H-filter inlet is reduced below 1:1, the concentration of *E. coli* in the gradient channel is reduced as well (nearly proportionally). As compared with the *E. coli* suspension fed to the cell inlet, the suspension in the gradient channel is normally diluted approximately threefold (as judged by counting individual *E. coli* in the field of view), corresponding to $OD_{600} \approx 0.03$. Another added benefit of the H-filter is the refreshment of the *E. coli* medium. As a result of the cross-channel diffusion of motile cells, >50% of the *E. coli* medium content is replaced with fresh motility buffer as shortly as ~30 s before the beginning of the thermotaxis assay (the time in flow between the outlet of the H-filer and the inlet of the gradient channel). The refreshment of the medium immediately before the thermotaxis assays, low concentration of *E. coli* in the medium, the absence of major chemoattractants and of rapidly metabolized nutrients in the medium, and the relatively short duration of the assays (~7 min) were expected to facilitate the establishment of well-defined, reproducible medium conditions during the thermotaxis assays.

Temperature control and video microscopy setup

The thermotaxis experiments were conducted on an inverted fluorescence microscope (Nikon TE2000) in an environmental enclosure. The temperature in the enclosure was set at $T_e = 34$°C, the same as the *E. coli* culture growth temperature, and to further standardize the experimental conditions, the reservoir with *E. coli* was placed inside the enclosure. In experiments with relatively steep temperature gradients, corresponding to large temperature differences between T_h and T_c, the temperature at the middle of the gradient channel (average between T_h and T_c) was usually close to T_e. Therefore, the effect of the heat exchange between the microfluidic device and the air beneath the device upon the temperature profile in the gradient channel was minimal. To circulate cold and hot water through the two 1-mm-deep circulation channels, we used two separate circulation water baths, which were set to different temperatures. The flow rates were ~2.0 mL/s. To accurately assess the temperatures inside the circulation channels, the tubing lines connected to their inlets and outlets had in-line thermistors, which were placed at equal short distances from the inlets and outlets (and were precalibrated in a temperature-controlled water bath). The temperature in a circulation channel was calculated as the average between the temperature readings of the thermistors upstream of the inlet and downstream from the outlet (33). The largest difference in the readings between the upstream and downstream thermistors was ~1.0°C (measured for the line with $T_h = 67$°C in the experiment with $T_c = 7$°C).

Micrographs of *E. coli* in the gradient channel were taken with a 20×/ 0.75 Nikon objective (1 mm working distance), 0.55× video coupler, and a 2/3-inch digital black-and-white CCD camera (Basler a102f) under oblique brightfield illumination (to enhance the contrast). The field of view was 550 μm along the gradient channel and covered the entire width of the channel. The objective was focused at the midplane of the channel (50 μm from the bottom). To detect individual bacteria, two consecutive micrographs

were taken with a short time interval ($\sim$133 ms). A certain constant value was then added to all pixels of the first micrograph, and the second micrograph was digitally subtracted from it. In the resulting image, regions without cells appeared as a uniform gray background (at the level of the added pixel value with some noise), whereas each cell produced a pair of a dark and bright spots at positions where the cell was located in the first and second micrographs (Fig. 1, *B* and *C*). Because of the motion of cells with the flow, these locations were on average $\sim$6 μm apart along the flow direction (the product of the maximal flow velocity of $\sim$45 μm/s and the 133 ms interval). The image was processed with a homemade code in MATLAB (The MathWorks, Natick, MA) that used smoothing and thresholding to identify cells and their locations. Because of the relatively large depth of the gradient channel, the defects at the top and bottom of the channel (and bacteria stuck to the top and bottom) were out of focus and had little effect on the uniform gray background. The pairs of micrographs were taken with an interval of $\Delta t = 5$ s, corresponding to an $\sim$150-μm average displacement along the flow, which is $\sim$1/3.6 of the size of the field of view. However, within this interval, cells were expected to move a distance of as much as $\sqrt{2D\Delta t} = 60$ μm in the vertical direction, much greater than the depth of field of the video microscopy setup ($\sim$5 μm). Therefore, a great majority of cells that were identified in the images were counted only once.

To visualize the temperature profile in the gradient channel at various T_h- and T_c-values, we used a 10-ppm solution of HPTS (8-hydroxypyrene-1,3,6-trisulfonic acid) fluorescent dye in 50 mM Tris buffer (pH 7.6 at 25°C), which was perfused through the gradient channel. The pH of Tris buffer decreases with temperature, and HPTS becomes less fluorescent as the pH of the medium decreases, resulting in a reduction of fluorescence of the HPTS solution by $\sim$1.7% per 1°C. Fluorescence illumination was derived from a 455-nm LED. We used a GFP filter and a 20$\times$/0.75 objective focused at the gradient channel midplane. Fluorescence background was accounted for by taking micrographs of the gradient channel with plain buffer in it. Flat-field correction was performed by taking fluorescence micrographs of the gradient channel with the HPTS solution without temperature gradient applied (no water in the circulation channel) and fitting the cross-channel distribution of brightness with a polynomial. To convert the local intensity of HTPS fluorescence in the gradient channel into local temperature, we measured cross-channel profiles of fluorescence at different spatially uniform temperatures. To this end, both circulation channels were connected to the same bath ($T_h = T_c$), which was consecutively set to temperatures of 25, 30, 35, 40, and 45°C. After the proper background subtraction and flat-field correction, the cross-channel fluorescence profiles in an $\sim$340-μm-wide central region of the channel were practically flat at all temperatures (fluorescence profiles were distorted near the side walls because of the combined effects of finite channel depth, relatively large numerical aperture of the objective, and reflections from the channel walls).

RESULTS

Temperature gradients

In our early experiments, the temperature gradients deduced from the measured cross-channel fluorescence profiles of a 10-ppm solution of HPTS in Tris buffer were as much as $\sim$1.4-fold steeper than the temperature gradients predicted by our numerical simulations for the same values of T_c and T_h (Fig. S2). We assumed it was because the temperature gradient applied across the gradient channel caused thermophoresis of HPTS, resulting in reduced concentrations of HPTS at higher temperatures and increased concentration at lower temperatures and in a larger slope of the fluorescence profile (as compared with the case of a uniform concentration of HPTS and its local fluorescence affected by

the temperature only). To test for possible effects of thermophoresis, we first, used the HTPS solution in Tris buffer to experimentally verify that, as our numerical simulations indicated, steady-state temperature profiles in the gradient channel were established very rapidly (within $<$10 s; Fig. S3 *A*). After that, we used a 10-ppm solution of HPTS in phosphate buffer (pH 7.4 at 25°C), which had a much lower temperature sensitivity of its pH (0.002 units per 1°C vs. 0.03 units per 1°C for Tris buffer). Profiles of fluorescence of this solution were measured at residence times in the temperature gradient, t_{res}, ranging from 10 to 320 s (Fig. S3 *B*). The results showed a cross-channel gradient of fluorescence gradually building up and becoming nearly steady at $\sim$4.5% per 300 μm or $\sim$0.6% per 1°C by t_{res} of $\sim$160 s, with the transition to the steady gradient 50% complete after $\sim$40 s (Fig. S3 *B*). Numerical simulations with the diffusion coefficient of HPTS taken at 450 μm^2/s and the effect of thermophoresis represented by a spatially uniform drift velocity across the gradient channel, $v_d = 0.07$ μm/s, showed a transition from the initial uniform concentration profile to the experimentally measured steady-state gradient ($\sim$4.5% per 300 μm). The transition was 50% complete after $\sim$52 s, in good agreement with the experimental data, thus supporting the assumption that thermophoresis caused a gradient of HPTS concentration across the gradient channel. The 0.6% decrease in concentration of HPTS per 1°C increase in temperature was close to 4/10 of the decrease in fluorescence of HTPS in Tris buffer per 1°C (at spatially uniform temperature). Hence, the experimentally observed $\sim$1.4-fold enhancement (versus numerical simulations) of the effect of temperature gradient on the slope of the fluorescence profile of HPTS in Tris buffer in the gradient channel was, indeed, most likely due to thermophoresis.

To minimize the effect of thermophoresis on the fluorescence of HPTS in Tris, we used the fact that the time of establishment of a stable temperature gradient across the gradient channel is only $\sim$1 s (based on our numerical simulations), which is much shorter than the characteristic time of cross-channel thermophoresis ($\sim$100 s). We measured profiles of fluorescence of HTPS in Tris at $t_{res} \approx 10$ s (we first started flow through the gradient channel at a very high speed, then stopped the flow and waited for 10 s), such that the temperature gradient was expected to be fully established, whereas the nonuniformity of concentration of HTPS was expected to be minimal (cf. Fig. S3 *B*). The measurements were performed for three sets of the T_c- and T_h-values: 19 and 59°C, 14 and 54°C, and 14 and 64°C (Fig. 2). In all cases, the temperature profiles in the 340-μm-wide central region of the channel were nearly linear with slopes, $\Delta T/\Delta x$, proportional to the difference $T_h - T_c$, $\Delta T/\Delta x = a(T_h - T_c)$, with the prefactor $a = 0.89$ mm^{-1} in a good agreement with the numerical simulation prediction of $a = 0.89$ mm^{-1} (Fig. S2). Therefore, we adopted the formula $\Delta T/\Delta x = a(T_h - T_c)$ with $a = 0.89$ mm^{-1} for
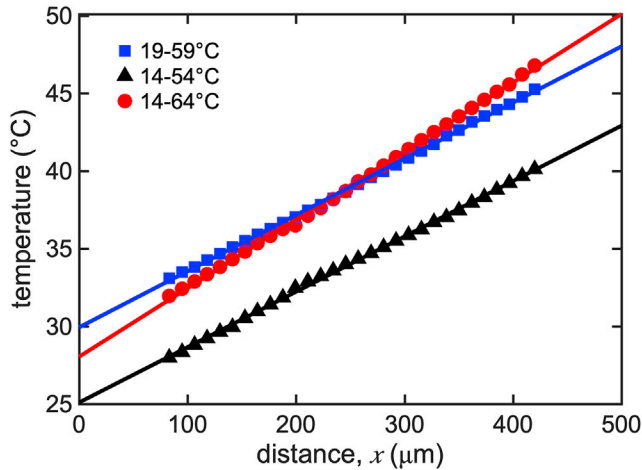
FIGURE 2 Temperature of a solution of HPTS in Tris buffer in the gradient channel as a function of the distance, x, from the left (cold) wall at three different combinations of temperature of water in the cold and hot circulation channels, T_c and T_h. The values of T_c and T_h were, respectively, 19 and 59°C (blue squares), 14 and 54°C (black triangles), and 14 and 64°C (red circles). The temperature was calculated from the local intensity of fluorescence of HPTS, using cross-channel fluorescence profiles of the same solution at spatially uniform temperatures for calibration. The color-matching straight lines are linear fits to the experimental data, $T(x) = T_0 + a(T_h - T_c)x$, with the coefficients a of 0.90, 0.90, and 0.88 mm^{-1} for the blue, black, and red lines, respectively. The average value of a for the three data sets was 0.89 mm^{-1}, in good agreement with $a = 0.89$ mm^{-1} as predicted by the numerical simulations. To see this figure in color, go online.

calculations of temperature gradients in our thermotaxis experiments. In what follows, we report cross-channel temperature profiles in terms of the temperatures T_l and T_r at the left and right wall of the gradient channel, which are adjacent to the cold and hot circulation channel, respectively. Based on our numerical simulations (Fig. S2), we calculated these two temperatures as $T_l = T_c + 0.28(T_h - T_c)$ and $T_r = T_h - 0.28(T_h - T_c)$.

Thermotaxis in shallow, narrow-range gradients

We first studied the thermotaxis of E. coli in two shallow thermal gradients with $\Delta T/\Delta x = 8.9$°C/mm, one with $T_l = 36$°C and $T_r = 40$°C and the other one with $T_l = 39$°C and $T_r = 43$°C (Fig. 3). The distributions of E. coli across the gradient channel were assessed at the downstream end of the channel (11 mm from the beginning). The experiments were run for ~30 min after E. coli suspension was first fed into the microfluidic devices, with an average of 5000 cells analyzed per experiment. Each of the two experiments was performed three times ($N = 3$). An obvious feature of both distributions is that they are relatively flat, with only approximately twofold difference between the highest and lowest cell densities across the gradient channel. Nevertheless, there is a clear bias toward higher temperatures in the 36–40°C gradient, implying thermophilic
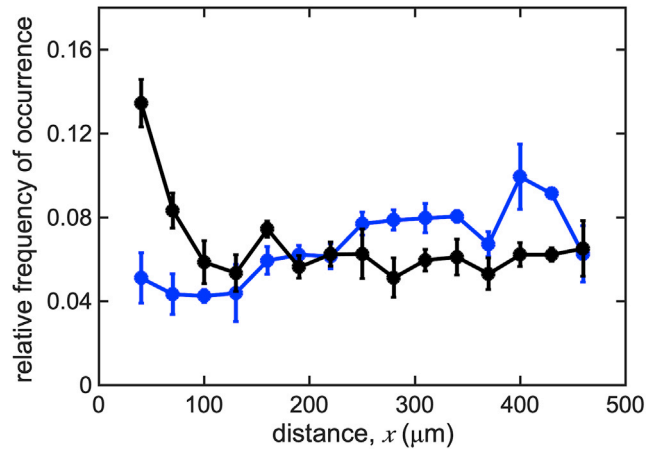

FIGURE 3 Distributions of E. coli cells across the gradient channel in two shallow gradients, both with $\Delta T/\Delta x = 8.9$°C/mm, with $T_l = 36$°C and $T_r = 40$°C (blue circles and blue line) and with $T_l = 39$°C and $T_r = 43$°C (black circles and black line). Relative frequencies of occurrence over a cross-channel distance, Δx, of 20 μm are plotted versus distance from the left (cold) wall of the gradient channel. For each set of conditions, each data point is an average over three separate experiments ($N = 3$), with cross-channel positions of 3000–5000 cells analyzed in each experiment. Error bars are the standard deviation for the three experiments. To see this figure in color, go online.

behavior of E. coli in this temperature range. The temperature bias in the 39–43°C gradient is weaker but still statistically significant, suggesting cryophilic behavior of E. coli in this temperature range. This reversal of behavior from thermophilic to cryophilic appears to be reasonable in view of the fact that the E. coli growth rate (in a rich medium) sharply drops at temperatures above ~43°C. It is also worth noting that there was no sign of aggregation of E. coli at any intermediate temperatures in either of these shallow gradients.

Thermotaxis in steep, wide-range gradients

We studied thermotaxis of E. coli in steeper temperature gradients, with temperature profiles in the gradient channel covering relatively broad ranges both below and above the putative aggregation temperature of 37°C. We performed four different experiments (with $N = 3$ repeats of each) with the values of T_l and T_r of, respectively, 32 and 46°C, 30 and 48°C, 28 and 50°C, and 24 and 50°C (Fig. 4). The temperature gradients were $\Delta T/\Delta x = 27$, 36, 45, and 53°C/mm, respectively. The salient features of cross-channel distributions of E. coli in all of these experiments are well-pronounced single peaks and large ratios between the maximal and minimal local densities of cells, clearly showing that in these gradients, E. coli aggregate at certain intermediate temperatures. To our surprise, however, we found that the aggregation temperatures (temperatures at the peaks of the distributions) were not the same for different gradients, but rather monotonically decreased as the gradient became steeper: from ~40°C at
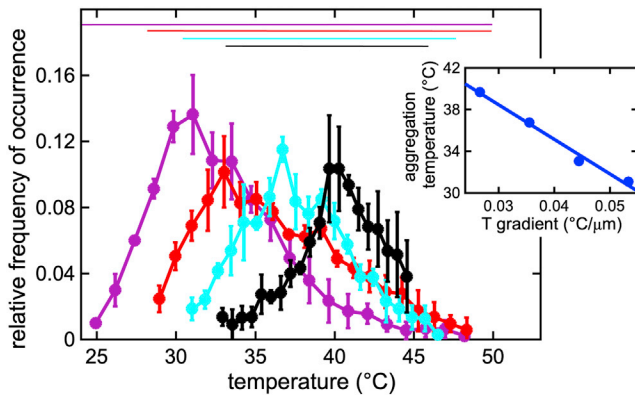
FIGURE 4 Distributions of *E. coli* cells across the gradient channel in four steep gradients, with the values of T_l, T_r, and $\Delta T/\Delta x$ of, respectively, 32, 46, and 27°C/mm (*black circles* and *line*); 30, 48, and 36°C/mm (*cyan circles* and *line*); 28, 50, and 45°C/mm (*red circles* and *line*); and 24, 50, and 53°C/mm (*magenta circles* and *line*). Relative frequencies of occurrence over a cross-channel distance, Δx, of 25 μm are plotted versus local temperature. For each set of conditions, each data point is an average over three separate experiments ($N = 3$), with cross-channel positions of 3000–5000 cells analyzed in each experiment. Error bars are the standard deviations for the three experiments. Color-matching horizontal bars at the top show the ranges of temperature in the four gradients. The inset shows the aggregation temperature (temperature at the peak of the distribution) versus slope of the temperature profile, $\Delta T/\Delta x$, at the four sets of experimental conditions. Straight line is a linear fit with a slope of –0.35 mm [−0.35°C/(°C/mm)]. To see this figure in color, go online.

$\Delta T/\Delta x = 27$°C/mm to ~37°C at 36°C/mm, to ~33°C at 45°C/mm, and to ~30°C at 53°C/mm.

To verify that the aggregation in the temperature gradients is not a transient effect depending on the residence time in the gradient channel, t_{res}, we repeated the experiment with the steepest gradient, 24–50°C ($\Delta T/\Delta x = 53$°C/mm), while measuring the cross-channel distributions of *E. coli* at two different positions: near the end of the gradient channel (the regular position), with $t_{res} = 360$ s, and at two-thirds of the way from the beginning to the end, with $t_{res} = 240$ s. The two distributions (Fig. S4) were similar, both having peaks at ~30°C, indicating that the aggregation around this temperature is stable, once established, and persists for at least 120 s.

To test the effect of the H-filter upon distributions of *E. coli* in the temperature gradients, we repeated experiments with the least steep gradient ($T_l = 32$°C, $T_r = 46$°C, and $\Delta T/\Delta x \approx 27$°C/mm) with a modified setup in which the H-filter was effectively disabled. The cross-channel distribution of *E. coli* observed in these experiments (Fig. S5) had a peak at a temperature of ~38.5°C, nearly the same as the aggregation temperature of ~39.5°C in the experiments with the functional H-filter (*black symbols* in Fig. 4). With the disabled H-filter, however, the ratio of the *E. coli* concentration at the peak to their average cross-channel concentration was lower than with the functional H-filter. This change in the distribution was consistent with the expected effect of the presence of nonmotile cells.

As another control, we repeated the experiments with the least steep gradient (now with the regular functional H-filter) with cells of a $\Delta cheA$ line of *E. coli*, which are not capable of chemotaxis because of the deletion of the gene encoding for the CheA kinase. The cross-channel distribution of *E. coli* from this cell line (Fig. S6) did not exhibit a peak at an intermediate temperature, indicating that the aggregation at intermediate temperatures observed with RP437 *E. coli* (Fig. 4) depended on the chemotaxis signal transduction pathway and was not a result of temperature dependence of the swimming velocity.

Next, we tested whether the aggregation temperature of RP437 *E. coli* depends on the steepness of the gradient (a local property of the temperature field) or on the entire range of temperatures that *E. coli* are presented with and are allowed to explore. To this end, we first performed another experiment with $\Delta T/\Delta x = 36$°C/mm (cf. Fig. 4), but with the interval T_l–T_r shifted down by 5°C, from 30 to 48°C to 25 to 43°C. When plotted in the coordinates of the frequency of occurrence (density of bacteria) versus temperature, the two distributions had peaks at temperatures that differed by ~1°C (Fig. 5 A). On the other hand, when the abscissa was changed to the distance from the left (cold) channel wall (Fig. 5 B), the two distributions had peaks as far as 120 μm apart (~0.25 of the channel width). Next, we performed an additional experiment with $\Delta T/\Delta x = 45$°C/mm (cf. Fig. 4), but with the interval T_l–T_r shifted down by 5°C, from 28 to 50°C to 23 to 45°C. Again, when plotted in the coordinates of the frequency of occurrence versus temperature, the distributions of *E. coli* had peaks at temperatures that differed by only ~1°C (Fig. 5 C). On the other hand, when the abscissa was changed to the distance from the left channel wall (Fig. 5 D), the peaks of the two distributions were ~100 μm apart. It is worth noting, however, that there appears to be systematic shifts between the two distributions in Fig. 5 A and the two distributions in Fig. 5 C at temperatures away from their peaks. Conversely, the distributions in Fig. 5, B and D somewhat converge toward the channel sidewalls, with bacterial densities tending to reach zero at the physical boundaries (channel walls) rather than at certain temperatures. The results of these two experiments indicate that, in the temperature ranges we explored, the aggregation temperatures of *E. coli* strongly depend on the steepness of the gradient, although depending relatively weakly on the total range of temperatures that cells are allowed to explore. On the other hand, the detailed shapes of the distributions of *E. coli* in temperature gradients relatively strongly depend on the range of temperatures in the region of space that cells are confined to.

DISCUSSION

We used a microfluidic device to study thermotaxis of *E. coli* in a variety of linear temperature gradients, which
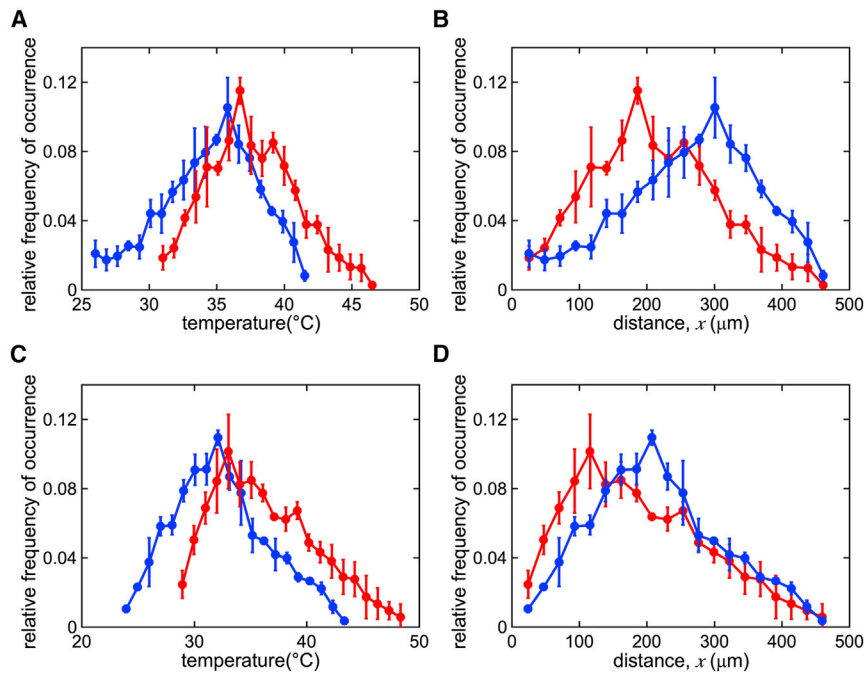
FIGURE 5 Distributions of *E. coli* cells across the gradient channel in cross-channel temperature profiles with identical slopes, $\Delta T/\Delta x$, but different temperature ranges, T_l–T_r. (*A*) and (*B*) $\Delta T/\Delta x = 36°C/mm$ with $T_l = 25°C$ and $T_r = 43°C$ (*red circles* and *line*) and with $T_l = 30°C$ and $T_r = 48°C$ (*blue circles* and *line*). (*C*) and (*D*) $\Delta T/\Delta x = 45°C/mm$ with $T_l = 23°C$ and $T_r = 45°C$ (*red circles* and *line*) and with $T_l = 28°C$ and $T_r = 50°C$ (*blue circles* and *line*). In (*A*) and (*C*) relative frequencies of occurrence over a cross-channel distance, Δx, of 25 μm are plotted versus local temperature. In (*B*) and (*D*) the same relative frequencies of occurrence as in (*A*) and (*C*), respectively, are plotted versus the distance, *x*, from the left (*cold*) channel wall. For each set of conditions, each data point is an average over three separate experiments ($N = 3$), with cross-channel positions of 3000–5000 cells analyzed in each experiment. Error bars are standard deviation for the three experiments. To see this figure in color, go online.

spanned nearly an order of magnitude in steepness, from 9 to 53°C/mm, and were all generated across the same 500-μm-wide channel. The microfluidic device and experimental setup have a number of features that facilitate carrying out consistent, reproducible, and informative thermotaxis experiments. The arrangement with continuous flow of an *E. coli* suspension through a long channel with a cross-channel temperature gradient and with the assessment of the *E. coli* distribution at the channel end makes it possible to analyze a large number of cells per experiment, even when the cell density is relatively low ($OD_{600} = 0.03$). Low cell density leads to low rate of global changes in the medium composition caused by cellular metabolism and also minimizes cell-to-cell interactions mediated by the local uptake and secretion. Because of the low cell density and high gas-permeability of the microfluidic chip (which is made of polydimethylsiloxane), *E. coli* respiration is not expected to cause any substantial reduction in the oxygen tension in the gradient channel (35). To further reduce the effects of changes in the medium composition during the thermotaxis assays, we had *E. coli* suspended in motility buffer without major chemoattractants or rapidly metabolized nutrients, with glycerol as the energy source. In our tests, we could not detect any growth of *E. coli* strain RP437 in this motility buffer.

The proposed experimental setup, with a relatively deep gradient channel, $h = 100$ μm, also makes it easy to visualize and detect *E. coli* cells without fluorescent markers by taking two brightfield micrographs at the midplane of the channel with a short time interval and digitally subtracting the second micrograph from the first one. We note that the ~18-s time of passage of bacterial suspension through

the field of view of the video microscopy setup (flowing at 30 $\mu m/s$ across 550 μm) is longer than the characteristic time of the diffusion-like motion of *E. coli* along the channel depth, $h^2/(2D) = 12.5$ s, making it possible to sample nearly all cells passing through the gradient channel. In our experiments, consecutive pairs of micrographs were taken with an interval of 5 s, which is much longer than the characteristic time of motion of bacteria through a horizontal layer with the thickness of the depth of field of the optical setup, $\Delta z \approx 5$ μm (the layer at the channel midplane, where the images of bacteria were sharp enough to enable their reliable identification). Therefore, each pair of micrographs provided data on a sample with a subpopulation of bacteria that was largely different from subpopulations in all other samples. On the other hand, the entire population of bacteria in the 550-μm-long segment of the channel is equivalent to about $h/\Delta z \approx 20$ samples, whereas we only sampled it ~3.6 times during the ~18-s time of passage through the field of view. Hence, in our experiments, the population of bacteria in the gradient channel was undersampled by a factor of ~5.5.

Another important feature of the experimental setup is the microfluidic H-filter (34) upstream of the gradient channel. This filter does not allow any nonmotile *E. coli* cells (e.g., cells with flagella damaged during centrifugation and resuspension) to enter the gradient channel, thus improving the consistency and reproducibility of the experimental results and increasing the visibility of the peaks of cell density distribution. Notably, in all experiments with *E. coli* aggregation at intermediate temperatures, the ratios between the maximal and minimal cell densities were >10 (Figs. 4 and 5), whereas in the experiments on *E. coli* aerotaxis

(29), in which no H-filter was used, cell densities at peaks of the distributions were never more than fivefold greater than the minimal densities. The H-filter also enables real-time adjustment of the concentration of *E. coli* in the gradient channel, and last, but not least, it exchanges >50% of the content of the medium to that of fresh motility buffer as shortly as 30 s before the beginning of the thermotaxis assay. This refreshment of the medium (together with the fact that it is a defined minimal medium with a low nutrient consumption rate), the low concentration of *E. coli* in the medium, the high oxygen permeability of the device, and the relatively short residence time of *E. coli* in the gradient channel (~6 min) all contribute toward the establishment of well-defined conditions during the thermotaxis assays.

Rapid circulation of temperature-controlled water through two deep, closely spaced parallel channels (Fig. 1) is a flexible and versatile way to generate temperature gradients. Temperature gradients in the gradient channel always have the same, near-linear shape (Fig. S2), and both the steepness of the gradient and the range of temperatures that cells are presented with can be varied in broad ranges. Moreover, they both are linear functions of the temperatures of the circulated cold and hot water, T_c and T_h: $\Delta T/\Delta x = 0.89$ mm^{-1} $\times (T_h - T_c)$ and from $T_l = T_c + 0.28(T_h - T_c)$ to $T_r = T_h - 0.28(T_h - T_c)$, respectively. Hence, all parameters of the temperature gradients can be readily calculated from the measured values of T_c and T_h, and the gradients do not need to be calibrated for each individual thermotaxis experiment. In addition, the temperature gradients in the gradient channel are largely one-dimensional, with relatively little temperature changes along the channel depth. (Our numerical simulations indicated that a temperature change along the channel depth, h, is always <12% of the temperature variation along the same distance of 100 μm in the cross-channel direction).

We believe that for the purposes of experiments on thermotaxis, this temperature gradient generation technique compares favorably with the temperature gradient generation using an infrared laser emitting light with a wavelength of ~1480 nm that is absorbed by water. In this latter technique, the temperature profiles are always nonlinear, and variations of temperature along the channel depth may be comparable with temperature variations in the direction of the main gradient, which is along the radius of the laser beam, making the temperature gradients effectively three-dimensional (from numerical simulations; data not shown; the laser-generated temperature profiles can also be viewed as two-dimensional along the *r*- and *z*-directions in the cylindrical coordinates). In addition, this technique is incompatible with the continuous perfusion setup used in our study, thus only enabling a relatively low data collection rate, especially in experiments with low cell densities.

Our measurements of the cross-channel temperature profiles showed that, whereas the assessment of spatially uniform temperature using a solution of temperature-sensitive fluorescent dye is straightforward, the results of measurements of temperature gradients with such a fluorescent solution may be misleading because of the dye thermophoresis. Specifically, our experiments with HPTS in phosphate buffer (which has a very weak dependence of pH on temperature) indicate that thermophoresis across the 500-μm-wide gradient channel generates a gradient of HPTS concentration of ~0.6% per 1°C gradient of temperature. The intensity of fluorescence of the solution of HPTS in Tris buffer, which we used to visualize temperature profiles across the gradient channel, decreases by ~1.7% per 1°C (when temperature is spatially uniform). After an HPTS gradient driven by thermophoresis is fully established, the ~0.6% per 1°C change in fluorescence due to thermophoresis is added to the ~1.7% per 1°C change due to the inherent temperature dependence of fluorescence. As a result, the fluorescence gradient becomes ~1.4-fold steeper than the gradient measured before the thermophoresis is allowed time to change the local concentrations of HPTS. It is worth noting that we only discovered this effect because the disagreement between the temperature profiles obtained from our numerical simulations and the fluorescence profiles of HPTS in Tris measured in our early tests (with ~300 s allowed for thermophoresis) was too large to be explained by experimental errors.

We further note that, if the measured effect of thermophoresis in temperature gradients on spatial distributions of concentration of HPTS, 0.6% per 1°C, is similar to its effect on spatial distribution of nutrients (which are also small molecules), steep gradients of temperature are expected to generate appreciable gradients of nutrients. For example, when the temperature across the gradient channel varies by 27°C, as in one of our experiments, the concentration of nutrients in the medium would vary by ~16% across the 500-μm channel width. If some of those nutrients are major chemoattractants (e.g., glucose and amino acids present in reach media), such concentration gradients may cause considerable chemotaxis.

In our thermotaxis experiments, we used a motility buffer, which was a minimal medium with glycerol added as an energy (and carbon) source. Whereas spatial gradients of glycerol can cause *E. coli* chemotaxis (36), potential effects of the thermophoresis-driven gradients of glycerol on spatial distributions of *E. coli* are reduced by the virtue of glycerol being a relatively weak chemoattractant. Moreover, when added to a minimal medium at a concentration of 50 mM (the concentration in our thermotaxis medium), glycerol has been reported to have an effect of a repellant rather than attractant (37). There are very few literature data on thermophoresis of glycerol in water, but one would generally expect the gradient of glycerol concentration to be proportional to the temperature gradient and to be largely unchanged by shifts of the mean temperature (e.g., when T_l–T_r is shifted from 28 to 50°C to 23 to 45°C). That is, the glycerol concentration would always be higher at the

cold (or hot) wall of the gradient channel and thus driving the chemotaxis of *E. coli* toward the cold (or hot) wall, regardless of the mean temperature. In our experiments, we observed that the temperatures at which *E. coli* distributions have peaks are only weakly independent of the mean temperature in the T_l–T_r profile, whereas the locations of the peaks with respect to the gradient channel shift as the mean temperatures change (Fig. 4). This observation suggests that the measured distributions of *E. coli* are not affected by thermophoresis of nutrients or by chemotaxis that might result from the thermophoresis.

Our study has two major biological results. The first result is that in linear temperature profiles that span sufficiently broad ranges of temperature ($|T_r - T_l| \geq 14°C$) and are sufficiently steep ($\Delta T/\Delta x \geq 27°C/mm$), thermotaxis in a motility buffer leads to aggregation of *E. coli* at intermediate temperatures. Aggregation of *E. coli* at an intermediate temperature in a thermal gradient chamber was reported in a 1976 study by Maeda et al. (27). The evidence for aggregation presented in that study was a bright band in a micrograph of an $\sim 10^7$ cells/mL suspension of *E. coli* in phosphate buffer in an $\sim$10-mm-long thermal gradient chamber taken 2 h after the application of a gradient of 2.2°C/mm. It is not completely clear, however, whether this bright band, which had a width of $\sim$1 mm and appeared in a region with a mean temperature of 34°C, was directly related to thermotactic migration of *E. coli*. Net migration of *E. coli* in a thermal gradient can result from temperature dependence of the cell swimming speed (4,22), and after 2 h in a medium without energy sources, the swimming speed of *E. coli* was expected to substantially change, most likely in a temperature-dependent way. The authors noted that the bright band moved with time toward lower temperatures and that it was likely due to an oxygen gradient (27). One could expect such a gradient to result from the temperature- and cell-density-dependent cumulative respiration of *E. coli* in the gas-tight gradient chamber and to lead to some oxygen taxis and, potentially, contribute to the formation of bright band (high cell density region) on the micrograph.

Thermotactic aggregation of *E. coli* at intermediate temperatures was reported in two recent publications (15,29). Nevertheless, in both cases, the medium contained at least one of the two strong *E. coli* chemoattractants, serine and aspartate (or its analog MeAsp), which are chemoeffectors for the two most abundant receptors of *E. coli*, Tsr and Tar. Moreover, both articles explained the thermotactic aggregation of *E. coli* in terms of the combined effect of chemoattractants and ambient temperature upon changes in the methylation state of these two receptors in response to temperature changes. In (15) the case is made that the two receptors are essentially different and that Tsr always mediates thermophilic response but loses its sensitivity at high temperatures, whereas Tar mediates thermophilic response at low temperatures and cryophilic response at high temperatures. Therefore, whereas the aggregation

was only shown in a nutrient-rich medium (M9CG), it was also predicted to occur in a motility buffer. Nevertheless, an experimental test in a temperature gradient in motility buffer with a Δtsr line of *E. coli*, in which the entire thermotactic response was expected to be due to Tar receptor, did not reveal any clear intermediate temperature aggregation or switching from thermophilic to cryophilic behavior at intermediate temperatures (15).

In contrast, the extensive data on the intracellular signaling in *E. coli* in response to stepwise changes in temperature (obtained using FRET with fluorescent CheY and CheZ) in (29) indicate that the temperature responses of Tsr and Tar are surprisingly similar, both without chemoattractants and at equivalent concentrations of serine and MeAsp (when normalized to the sensitivity of the respective receptors to these chemoattractants). Based on these data, a detailed model was built in which the inversion of the response of *E. coli* from thermophilic to cryophilic (an essential element for the aggregation at an intermediate temperature) can only occur in the presence of either serine or aspartate (or MeAsp). However, the aggregation is not expected to occur in the absence of both chemoattractants or when they both are present at equivalent concentrations (29). Therefore, the observed aggregation of *E. coli* at intermediate temperatures in a motility buffer (without either of the two major chemoattractants) is a somewhat surprising result that cannot be readily explained in the framework of the model from (29). It is worth noting that our findings are consistent with the result of an experiment from (29) on *E. coli* in motility buffer in a temperature range of $\sim$27–33°C with $\Delta T/\Delta x$ of $\sim$18°C/mm (Figs. 2 and S2 *A* in (29)), which is steeper than the gradients in Fig. 3 but less steep than any of the gradients in Figs. 2 *E* and 4 of (29). That experiment showed no aggregation peak and a maximum cell density at the highest accessible temperature of $\sim$33°C, whereas we found thermal aggregation at $\sim$40°C in a gradient of $\sim$27°C/mm spanning the range of 32–45°C (the least steep gradient of those in Fig. 4; *black circles*).

The second major biological result of the study is that the temperature at which *E. coli* aggregate strongly depends on the gradient steepness, decreasing by as much as 10°C (from 40 to 30°C) as the gradient steepness increases twofold (from 27 to 53°C/mm). This dependence of the aggregation temperature on the gradient steepness was neither experimentally found nor theoretically predicted before, to our knowledge, making it very much surprising. To verify that this aggregation temperature shift is not an experimental artifact, we performed additional experiments in which we changed the ranges of temperature in the gradient channels while maintaining the gradient steepness unchanged (Fig. 5). Despite the temperature range shifts, the temperatures at which the distributions of density of *E. coli* peaked changed relatively little, by $\sim$1°C (on average) for 5°C range shifts, whereas the physical locations of the density peaks moved across the gradient channel by as much as

120 μm (~0.25 of the gradient channel width). Therefore, our experimental results indicate that the reduction of the aggregation temperatures in steeper gradients is a real phenomenon.

We note that the thermal gradients of 27–53°C/mm in the experiments in which *E. coli* aggregation at intermediate temperatures was observed (Fig. 4) were all steeper than thermal gradients that *E. coli* cells are likely to encounter in their natural (or laboratory) environment. However, we believe this aggregation to be a manifestation of the well-documented behavior of avoidance of excessively high and low temperatures (14,29) that serves the purpose of finding optimal growth conditions and that *E. coli* has evolved for. Therefore, we consider the application of the steep gradients as an experimental tool to observe the natural behavior of *E. coli* under better controlled conditions (relatively short aggregation time of ~5 min) and with higher clarity (sharper aggregation peaks). On the other hand, given the low likelihood of *E. coli* encountering the gradients of 27–53°C/mm, we believe the observed reduction of the aggregation temperature with the gradient steepness to be a byproduct of the existing wiring of the temperature sensing (and swimming) signal transduction network rather than a type of behavior *E. coli* has specifically evolved for.

Unfortunately, we have not been able to propose a plausible mechanism explaining the reduction of the aggregation temperature with the steepness of the thermal gradient. It is worth noting, however, that in both experiments with temperature range shifts (Fig. 5, *A* and *C*), the temperatures of the density distribution peaks were lower for temperature ranges shifted down. Moreover, away from the peaks, the cell density distributions for different temperature ranges (and same gradient steepness) increasingly diverged when plotted against the temperature (Fig. 5, *A* and *C*) and converged when plotted against the position across the gradient channel (Fig. 5, *B* and *D*). Most conspicuously, cell densities near the gradient channel sidewalls (positions of 0 and 500 μm) were close to zero in all cases (Fig. 5, *B* and *D*). Notably, this dependence of the shapes of the cell density distributions is not readily reproduced by simple models, in which the motion of *E. coli* across the gradient channel is a biased random walk with a drift velocity that solely depends on the local temperature and temperature gradient (Fig. S7). These experimental observations and results of mathematical modeling suggest that the distributions of density of *E. coli* across the gradient channel do not solely depend of the steepness of temperature gradient but are also influenced by some physical effects of the channel sidewalls and, possibly, by the range of temperatures that cells are presented with and allowed to explore.

A plausible effect of the channel sidewalls is the loss of cells from the layer near the channel midplane, where cells are imaged and counted. This loss could be because of the sticking of cells to the sidewalls or some more intricate ef-

fect related to a different flow velocity pattern near the sidewalls as compared with the internal region of the channel, where the flow velocity is uniform over horizontal planes and has a parabolic profile along the vertical direction. To account for the cell loss, we repeated the numerical simulation of biased random walk toward the aggregation temperature (cf. Fig. S7) while changing the boundary conditions from zero flux (impermeable boundaries) to an outwards flux with a rate proportional to the concentration of cells at the boundaries. This new model (Fig. S8) qualitatively reproduced several major trends of the experimental data (Fig. 5) that were not captured by the model with impermeable walls (cf. Fig. S7). Specifically, for identical gradients and different temperature ranges, cell density distributions peaked at different temperatures (lower aggregation temperatures for temperature ranges shifted down; cf. Fig. 5, *A* and *C*) and converged toward the sidewalls when plotted against the position across the channel (cf. Fig. 5, *B* and *D*). It is worth noting that the assumption of the model about the cell loss is consistent with the experimental observation that the number of cells in the midplane of the gradient channel is reduced approximately threefold at the end of the channel as compared with the beginning of the channel.

To summarize, we used a specially designed microfluidic device and experimental setup to perform extensive series of experiments on thermotaxis of *E. coli* suspended in a motility buffer in a stable linear temperature profile across a microchannel. The experiments revealed the aggregation of *E. coli* at intermediate temperatures away from the sidewalls of the microchannel with the temperature gradient. Surprisingly, the aggregation temperatures decreased for steeper temperature gradients, an effect that we have not been able to find a plausible explanation for. Moreover, when plotted both against temperature and against position across the channel, the shapes of distributions of cell density in the temperature gradients changed when the range of temperatures was shifted, whereas the steepness of the gradient was left unchanged. These changes in the cell density distributions were not reproduced by a simple model with biased random walk. Taken together, our results indicate that *E. coli* thermotaxis is a complex phenomenon, which, in addition to the temperature gradient itself, is likely influenced by the range of temperatures that cells are allowed to explore, the geometry of the chamber that cells are confined to, and the flow pattern in the chamber.

SUPPORTING MATERIAL

AUTHOR CONTRIBUTIONS

C.-Y.Y. designed and built microfluidic devices and experimental setup, performed experiments, and wrote the manuscript. A.G. designed the study,

designed microfluidic devices and experimental setup, performed numerical simulations, and wrote the manuscript. J.W.-N. contributed to the design of the study and experimental techniques. M.E. designed and built microfluidic devices and experimental setup and performed experiments. E.R. and E.G. contributed to the design of experimental techniques and experimental setup. L.T. performed experiments and contributed to design and building of the experimental setup.

ACKNOWLEDGMENTS

REFERENCES

1. Brown, D. A., and H. C. Berg. 1974. Temporal stimulation of chemotaxis in *Escherichia coli*. *Proc. Natl. Acad. Sci. USA*. 71:1388–1392.

2. Macnab, R. M., and D. E. Koshland, Jr. 1972. The gradient-sensing mechanism in bacterial chemotaxis. *Proc. Natl. Acad. Sci. USA*. 69:2509–2512.

3. Schnitzer, M. J., S. M. Block, …, E. M. Purcell. 1990. Strategies for chemotaxis. *Symp. Soc. Gen. Microbiol*. 46:15–34.

4. Schnitzer, M. J. 1993. Theory of continuum random walks and application to chemotaxis. *Phys. Rev. E Stat. Phys. Plasmas Fluids Relat. Interdiscip. Topics*. 48:2553–2568.

5. Gegner, J. A., D. R. Graham, …, F. W. Dahlquist. 1992. Assembly of an MCP receptor, CheW, and kinase CheA complex in the bacterial chemotaxis signal transduction pathway. *Cell*. 70:975–982.

6. Hazelbauer, G. L., J. J. Falke, and J. S. Parkinson. 2008. Bacterial chemoreceptors: high-performance signaling in networked arrays. *Trends Biochem. Sci*. 33:9–19.

7. Sourjik, V. 2004. Receptor clustering and signal processing in *E. coli* chemotaxis. *Trends Microbiol*. 12:569–576.

8. Sourjik, V., and H. C. Berg. 2002. Receptor sensitivity in bacterial chemotaxis. *Proc. Natl. Acad. Sci. USA*. 99:123–127.

9. Shioi, J., C. V. Dang, and B. L. Taylor. 1987. Oxygen as attractant and repellent in bacterial chemotaxis. *J. Bacteriol*. 169:3118–3123.

10. Adler, M., M. Erickstad, …, A. Groisman. 2012. Studies of bacterial aerotaxis in a microfluidic device. *Lab Chip*. 12:4835–4847.

11. Adler, J., and W. W. Tso. 1974. "Decision"-making in bacteria: chemotactic response of Escherichia coli to conflicting stimuli. *Science*. 184:1292–1294.

12. Yang, Y., and V. Sourjik. 2012. Opposite responses by different chemoreceptors set a tunable preference point in *Escherichia coli* pH taxis. *Mol. Microbiol*. 86:1482–1489.

13. Zhuang, J., R. Wright Carlsen, and M. Sitti. 2015. pH-taxis of biohybrid microsystems. *Sci. Rep*. 5:11403.

14. Paster, E., and W. S. Ryu. 2008. The thermal impulse response of *Escherichia coli*. *Proc. Natl. Acad. Sci. USA*. 105:5373–5377.

15. Yoney, A., and H. Salman. 2015. Precision and variability in bacterial temperature sensing. *Biophys. J*. 108:2427–2436.

16. Mizuno, T., and Y. Imae. 1984. Conditional inversion of the thermoresponse in *Escherichia coli*. *J. Bacteriol*. 159:360–367.

17. Maeda, K., and Y. Imae. 1979. Thermosensory transduction in *Escherichia coli*: inhibition of the thermoresponse by L-serine. *Proc. Natl. Acad. Sci. USA*. 76:91–95.

18. Salman, H., and A. Libchaber. 2007. A concentration-dependent switch in the bacterial response to temperature. *Nat. Cell Biol*. 9:1098–1100.

19. Lee, L., T. Mizuno, and Y. Imae. 1988. Thermosensing properties of *Escherichia coli* tsr mutants defective in serine chemoreception. *J. Bacteriol*. 170:4769–4774.

20. Nara, T., L. Lee, and Y. Imae. 1991. Thermosensing ability of Trg and Tap chemoreceptors in *Escherichia coli*. *J. Bacteriol*. 173:1120–1124.

21. Nishiyama, S., S. Ohno, …, I. Kawagishi. 2010. Thermosensing function of the *Escherichia coli* redox sensor Aer. *J. Bacteriol*. 192:1740–1743.

22. Demir, M., and H. Salman. 2012. Bacterial thermotaxis by speed modulation. *Biophys. J*. 103:1683–1690.

23. Oleksiuk, O., V. Jakovljevic, …, V. Sourjik. 2011. Thermal robustness of signaling in bacterial chemotaxis. *Cell*. 145:312–321.

24. Wiegand, S. 2004. Thermal diffusion in liquid mixtures and polymer solutions. *J. Phys. Condens. Matter*. 16:R357–R379.

25. Duhr, S., and D. Braun. 2006. Why molecules move along a temperature gradient. *Proc. Natl. Acad. Sci. USA*. 103:19678–19682.

26. Salman, H., A. Zilman, …, A. Libchaber. 2006. Solitary modes of bacterial culture in a temperature gradient. *Phys. Rev. Lett*. 97:118101.

27. Maeda, K., Y. Imae, …, F. Oosawa. 1976. Effect of temperature on motility and chemotaxis of *Escherichia coli*. *J. Bacteriol*. 127:1039–1046.

28. Demir, M., C. Douarche, …, H. Salman. 2011. Effects of population density and chemical environment on the behavior of *Escherichia coli* in shallow temperature gradients. *Phys. Biol*. 8:063001.

29. Paulick, A., V. Jakovljevic, …, V. Sourjik. 2017. Mechanism of bidirectional thermotaxis in *Escherichia coli*. *eLife*. 6:e26607.

30. Ahmed, T., T. S. Shimizu, and R. Stocker. 2010. Microfluidics for bacterial chemotaxis. *Integr. Biol*. 2:604–629.

31. Kalinin, Y. V., L. Jiang, …, M. Wu. 2009. Logarithmic sensing in *Escherichia coli* bacterial chemotaxis. *Biophys. J*. 96:2439–2448.

32. Mao, H., P. S. Cremer, and M. D. Manson. 2003. A sensitive, versatile microfluidic assay for bacterial chemotaxis. *Proc. Natl. Acad. Sci. USA*. 100:5449–5454.

33. Vandelinder, V., A. C. M. Ferreon, …, A. Groisman. 2009. High-resolution temperature-concentration diagram of alpha-synuclein conformation obtained from a single Förster resonance energy transfer image in a microfluidic device. *Anal. Chem*. 81:6929–6935.

34. Brody, J. P., P. Yager, …, R. H. Austin. 1996. Biotechnology at low Reynolds numbers. *Biophys. J*. 71:3430–3441.

35. Polinkovsky, M., E. Gutierrez, …, A. Groisman. 2009. Fine temporal control of the medium gas content and acidity and on-chip generation of series of oxygen concentrations for cell cultures. *Lab Chip*. 9:1073–1084.

36. Rebbapragada, A., M. S. Johnson, …, B. L. Taylor. 1997. The Aer protein and the serine chemoreceptor Tsr independently sense intracellular energy levels and transduce oxygen, redox, and energy signals for *Escherichia coli* behavior. *Proc. Natl. Acad. Sci. USA*. 94:10541–10546.

37. Diao, J., L. Young, …, M. P. DeLisa. 2006. A three-channel microfluidic device for generating static linear gradients and its application to the quantitative analysis of bacterial chemotaxis. *Lab Chip*. 6:381–388.